J. Fluid Mech. (1965), *vol.* 23, *part* 2, *pp.* 209–228
Printed in Great Britain

Experiments on the wall-pressure history in shock-reflexion processes

By D. BAGANOFF

Graduate Aeronautical Laboratories, California Institute of Technology, Pasadena, California

(Received 4 January 1965)

The normal reflexion of a plane shock wave from a plane wall is investigated experimentally using a new pressure gauge which has a rise time of 0·1 μsec and no overshoot. Wall-pressure histories of 5 μsec duration can be obtained with the present version of this gauge. The experiments were conducted on the end wall of the GALCIT 17 in. diameter shock tube.

Experimental results for three aspects of the reflexion process are presented and discussed: (1) effect of a cold wall, (2) effect of a vibrationally relaxing gas, and (3) profile for a reflecting shock front.

It is concluded that the effect of a cold wall introduces a comparatively minor perturbation to the wall-pressure history, since the 'thickness' of the shock-front profile exhibited by the wall-pressure history is comparable to the 'thickness' of the incident shock front, as measured by a stationary observer, and the pressure jump across the profile is about 90 % of the theoretical value for a thermally insulated wall. Also, the wall-pressure history immediately behind the reflected shock front can be approximated by boundary-layer theory. The effect of a vibrationally relaxing gas was studied in carbon dioxide, and it is shown that the relaxation process behind the incident shock wave produces a large effect on the recorded pressure history, which provides a method for measuring the vibrational relaxation time in carbon dioxide at high temperatures.

1. Introduction

This paper describes an experimental investigation of the short-time pressure history on the end wall of a shock tube during and immediately following the reflexion of an incident shock wave. The wall-pressure data were obtained with a new pressure gauge (Baganoff 1964) which has a rise time of 0·1 μsec and no overshoot. Pressure histories of 5 μsec duration can be obtained with the present version of this gauge.

In the ideal case the wall-pressure history is merely a step, with a jump in pressure equal to the Rankine–Hugoniot value. The aim of the present work is to study the difference in the wall-pressure history between the ideal pressure step and the real case. The deviation from the ideal case can be divided into three relatively independent studies: the initial-shock-front profile due to viscosity and heat conduction; a negative pressure perturbation following the shock front due to the heat transfer to the cold end wall, and, on a larger

time scale, a relaxation in the wall pressure due to real gas effects (vibrational relaxation, dissociation, and ionization). Since all three phenomena depend on collision processes in the gas, the time scale for each effect can be compared with the collision time τ_c in the initial gas. Figure 1 describes the pressure history on the end wall for the different cases and indicates the magnitude of the respective time scale encountered in the experiments.

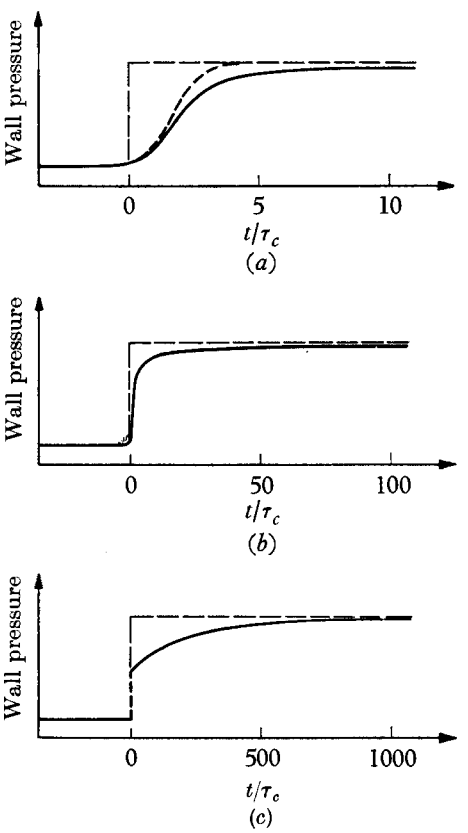

FIGURE 1. End-wall pressure history for various cases. (*a*) Shock-front profile; – – –, thermally insulated end wall; ——, cold end wall. (*b*) Effect of heat transfer to cold end wall. (*c*) Effect of vibrational relaxation.

The motivation for the present work stems primarily from the fact that the end-wall pressure is quite sensitive to relaxation processes in the driven gas, and this provides a new and convenient method for studying relaxation processes in gases. Also, it was found that the experimental method is capable of yielding information for higher temperatures and lower densities than attainable with a conventional optical interferometer.

The results of the study on the effect of heat transfer to the cold end wall are discussed first because of the importance of knowing when and to what degree the wall-pressure history for a relaxing gas would have to be corrected for heat-transfer effects. This phase of the investigation was carried out using argon and nitrogen as test gases, since they exhibit a more widely differing effect than some

of the other common gases. Then follows the discussion of the effect of a vibrationally relaxing gas. Carbon dioxide was employed as a test gas because of the Mach number limitation of the shock tube used ($M_s \approx 9$ for $p_1 \approx 50\,\mu$Hg) and the inherently short useful recording time of the pressure gauge. The final section presents the results of a study on the wall-pressure profile for a reflecting shock front in argon, nitrogen, and carbon dioxide.

2. Experimental method

The experiment was conducted on the end wall of the GALCIT 17 in. diameter low-pressure shock tube. The shock-tube facility has been described by Liepmann, Roshko, Coles & Sturtevant (1962); so only the features essential to the present experiment will be mentioned. These are the low leak rate, less than $0{\cdot}1\,\mu$Hg/h,

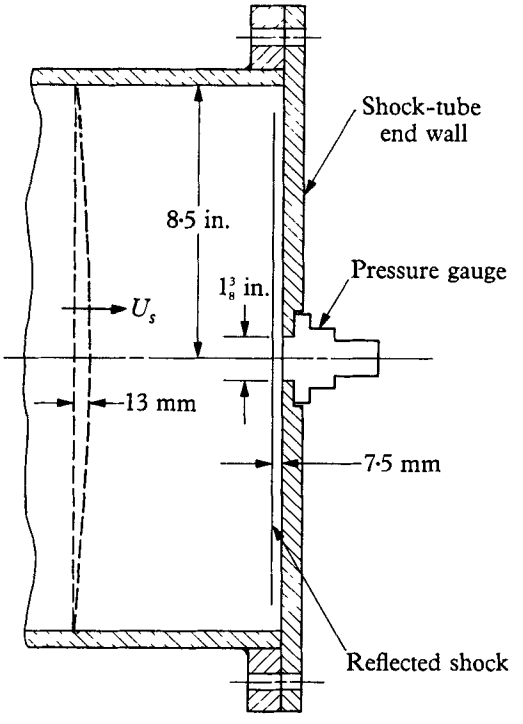

FIGURE 2. Relative dimensions of elements that affect the experiment. Incident shock: approximate shape for $p_1 = 50\,\mu$ Hg. Reflected shock: separation after 5 μsec assuming a plane incident shock and $M_s = 8$.

which made the task of holding the pressure level and purity level of the test gas to the value initially introduced into the driven section a relatively simple matter, and the large diameter of the shock tube which made possible, for the duration of the experiment, the realization of a good one-dimensional flow in the region near the axis of the shock tube, where the experiment was conducted.

The primary factors which alter the one-dimensional behaviour of the flow behind the reflected shock wave are the disturbances created by the boundary layer on the side wall of the shock tube (behind the incident shock) and the non-planar

surface of the incident shock wave (shock curvature). Because of the large diameter (17 in.) and the extremely short duration of the experiment ($\approx 5\,\mu$sec), the effect of the boundary layer disturbances behind the incident shock wave can be ignored. However, shock curvature can be important. Figure 2 presents a scale drawing of a portion of the shock tube at the end wall showing the relative dimensions of the maximum curvature of the incident shock wave, the maximum thickness of the reflected region for the experiment, and the pressure gauge. The incident shock wave was drawn using the data on shock curvature given by Liepmann & Bowman (1964). It is difficult to make a quantitative statement concerning the effect of shock curvature on the one-dimensional behaviour of the reflected flow. However, a rough estimate using the appropriate dimensions of the shock wave and the pressure gauge indicates that this can be ignored (Baganoff 1964).

The shock Mach number was determined by measuring the transit time of the shock wave between two thin-film heat gauges in the side wall of the shock tube at stations 20 and 70 cm from the end wall. The transit time (ranging from 200 μsec to 1200 μsec) was recorded on a microsecond counter (Berkeley 7260).

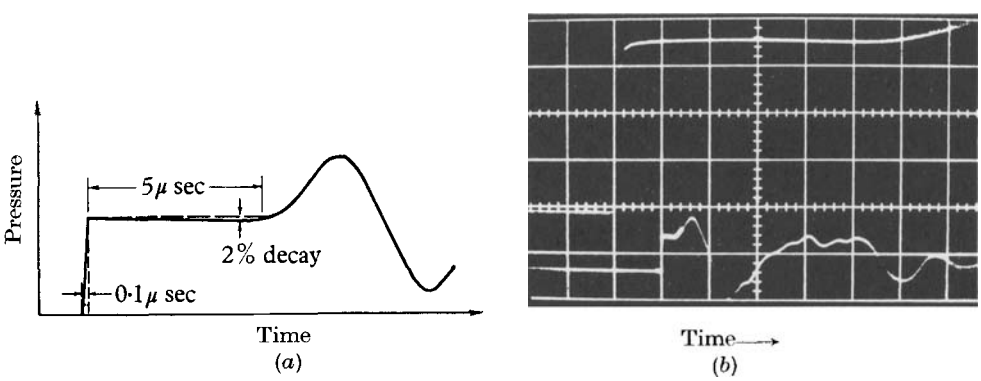

FIGURE 3. Response of the pressure gauge to a pressure step. (*a*) Diagrammatic description. (*b*) Oscillogram trace; driven gas, air; $p_1 = 760$ mm Hg, $M_s = 1{\cdot}19$; upper, 1 μsec/div; lower 20 μsec/div.

The pressure gauge was located on the centre line of the shock tube to minimize the effect of shock curvature. A small thin-film heat gauge, located 1 in. forward of the end wall and on a radius 6 in. from the pressure gauge, was used to trigger the oscilloscopes. This small separation between the end wall and the trigger gauge was found to be necessary for conveniently positioning the pressure trace on an oscillogram. Two Tektronix type 555 dual-beam oscilloscopes were used to obtain oscillograph traces of the pressure history for each run. All traces were recorded on type 47 Polaroid film (ASA 3000).

The pressure gauge used in the present series of tests has been described in a previous paper (Baganoff 1964). Several minor improvements were incorporated in the gauge. The sensitivity of the gauge was increased from 14 μV/mm Hg to 18·5 μV/mm Hg (based on a gauge voltage of 1 kV) by reducing the parasitic capacitance in the associated circuitry. The decay in the output signal (for an applied pressure step) was decreased to about 2 % by increasing the RC time

constant of the gauge-circuit combination. Figure 3 presents the response of the pressure gauge to a pressure step, and summarizes the important quantities associated with the performance of the gauge. It should be noted that the useful recording time of the gauge (for the present gauge diameter) is limited to the first 5 μsec after the onset of the pressure pulse. Therefore, the experimental data collected in these tests consists of 5 μsec samples of the initial portion of the pressure pulses.

The three gases used in the experiment (argon, nitrogen, and carbon dioxide) were taken directly from commercial cylinders.

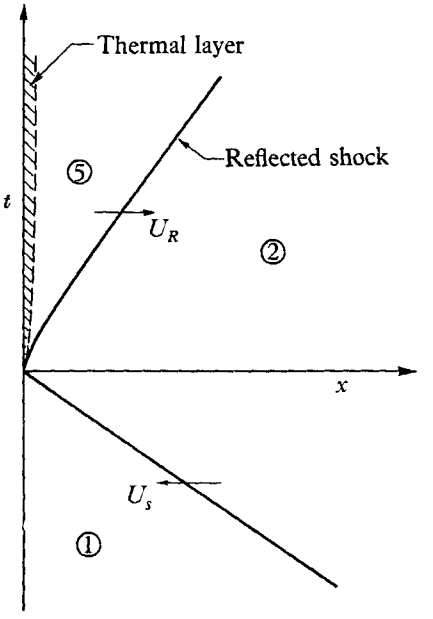

FIGURE 4. (x, t)-diagram for a shock reflecting from a cold wall.

3. Effect of a cold wall on the wall-pressure history

3.1. *Discussion*

The problem of the normal reflexion of a plane shock wave from a plane heat conducting wall has been treated by Goldsworthy (1959), Sturtevant & Slachmuylders (1964), and Clarke (1962). Goldsworthy's solution is based on a boundary-layer analysis and is therefore only valid for large time. The analysis divides the region behind the reflected shock wave into two parts: a boundary layer near the wall in which heat conduction plays a dominant role, and a region of inviscid linearized flow between the reflected shock and the boundary layer (see figure 4). The principal assumptions made are that the reflected shock wave can be replaced by a discontinuity, the thermal conductivity of the gas varies linearly with the temperature, and the quantities in the inviscid flow and the jump conditions across the reflected shock wave are perturbed only slightly from their ideal values.

The theoretical pressure perturbation p' on the end wall is given by equation

(55) of Goldsworthy's paper and can be written in the following dimensionless form:

$$p'/p_5 = -B(M_s)\,(1 - T_1/T_5)/\sqrt{\tilde{t}}, \tag{1}$$

where

$$\tilde{t} = t/\tau_5,$$

$$\tau_5 = (\gamma^2 k/\pi c_p \rho a^2)_5 = (\gamma^2 \mu/\pi Pr\, \rho a^2)_5,$$

T_1 is the temperature of the end wall, the quantities with the subscript 5 are the ideal values in region 5 (the reflected region), and $B(M_s)$ is a weak function of the incident-shock Mach number M_s and the ratio of specific heats γ; it accounts for the reflexion of perturbations from the reflected shock wave. If one neglects these reflexions $B(M_s) = 1$; actually it varies between the limits:

$$0{\cdot}928 < B(M_s) \leqslant 1 \quad \text{for} \quad \gamma = \tfrac{5}{3},$$
$$0{\cdot}793 < B(M_s) \leqslant 1 \quad \text{for} \quad \gamma = \tfrac{7}{5}.$$

(Two sign errors were found in equation (55) of the paper by Goldsworthy and were corrected in computing the function $B(M_s)$.) Since equation (1) was obtained by using boundary-layer theory, it is only valid for $\tilde{t} \gg 1$; the characteristic time τ_5 can be shown to be approximately equal to the collision time in region 5.

3.2. *Experimental results*

Figures 5 and 6 present several pressure traces for reflected shock waves in argon and nitrogen, showing the effects on the wall pressure due to heat transfer to the cold end wall. It is evident from an inspection of the pressure traces that the pressure perturbation is a small fraction of the total pressure jump and extends over a time scale somewhat greater than the time scale of the reflected shock front. Also a comparison of similar runs for argon and nitrogen shows that the effect of heat transfer is spread out over a longer time in argon than in nitrogen, indicating a dependence on the value of the thermal conductivity and the ratio of specific heats.

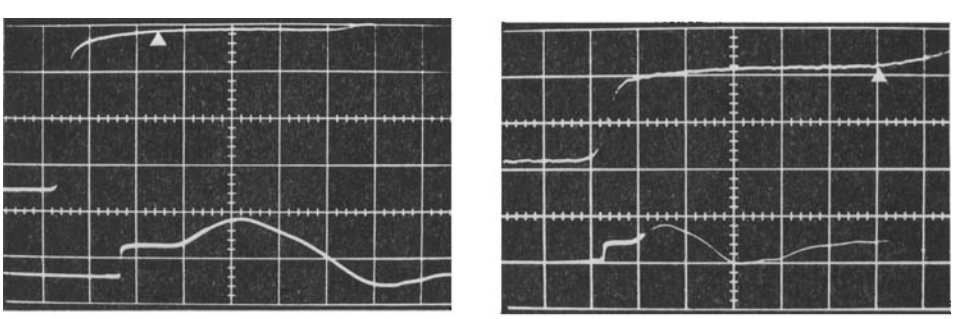

(*a*) (*b*)

FIGURE 5. Effect of a cold end wall on the wall-pressure history for reflected shocks in argon. (*a*) $p_1 = 1$ mm Hg, $M_s = 5{\cdot}64$; (*b*) $p_1 = 0{\cdot}5$ mm Hg, $M_s = 3{\cdot}25$. Both oscillograms: upper, 1 μsec/div; lower, 5 μsec/div.

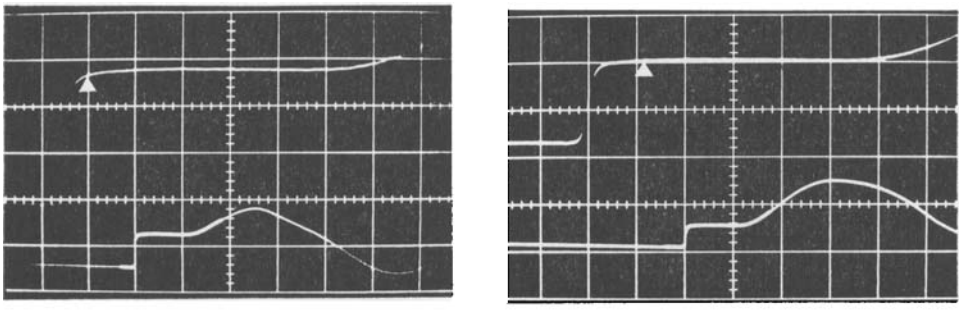

(*a*) (*b*)

FIGURE 6. Effect of a cold end wall on the wall-pressure history for reflected shocks in nitrogen. (*a*) $p_1 = 1$ mm Hg, $M_s = 5{\cdot}19$; (*b*) $p_1 = 0{\cdot}5$ mm Hg, $M_s = 3{\cdot}48$. Both oscillograms: upper, 1 μsec/div; lower, 5 μsec/div.

Although, in the traces of figures 5 and 6, the pressure perturbation appears to vary as $1/\sqrt{t}$, the accuracy and the range of the traces are, unfortunately, insufficient to test the law and determine how close to the shock front it breaks down. To make this check one would need the asymptotic pressure level to determine the pressure perturbation as a function of time; and in most cases the asymptotic pressure level cannot be determined from the trace, due to the 5 μsec

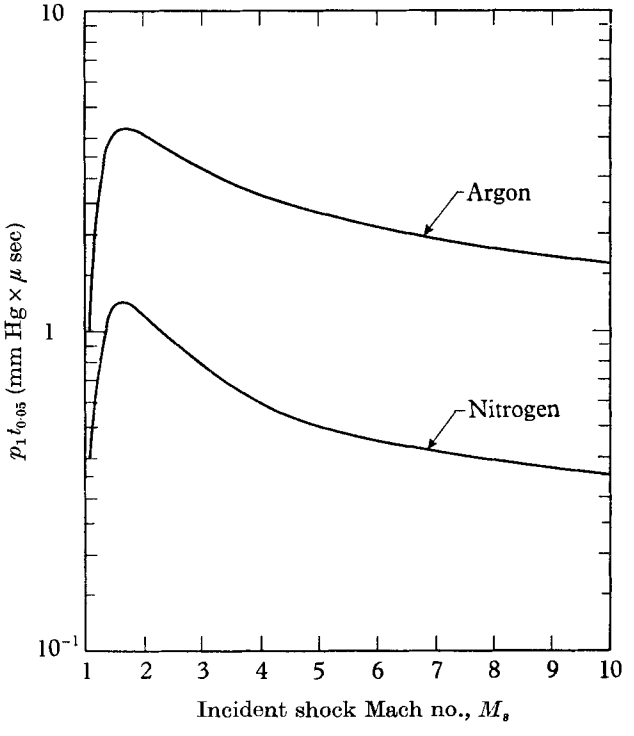

FIGURE 7. $p_1 t_{0\cdot05}$ for argon and nitrogen.

limitation of the present gauge. An alternative approach would be to determine the asymptotic pressure from the initial pressure, incident-shock Mach number, the theoretical pressure jump, and the gauge calibration. However, this would require an accuracy in the measurement of the initial pressure and in the determination of the gauge calibration which exceeds our present capability.

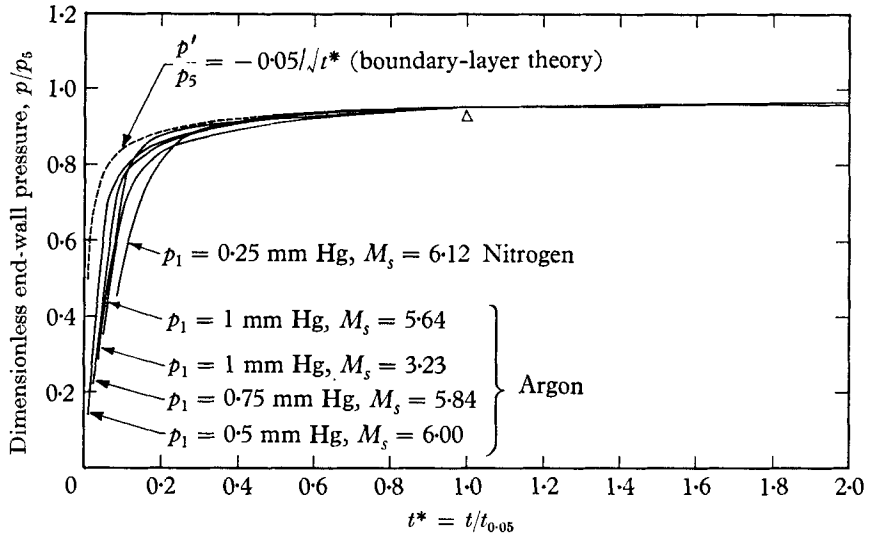

FIGURE 8. Non-dimensional plot of several experimental end-wall pressure histories.

Equation (1) and the data of Amdur & Mason (1958) were used to compute the time $t_{0{\cdot}05}$ at which a 5% pressure perturbation occurs. The quantity $p_1 t_{0{\cdot}05}$ is presented in figure 7 as a function of Mach number for argon and nitrogen. The figure shows a difference in $t_{0{\cdot}05}$ of roughly a factor of four between argon and nitrogen for the same initial pressure and incident Mach number.

The location of the theoretical 5% point is shown in figures 5 and 6 by a small triangle. (The time origin was arbitrarily placed at the intersection point determined by a line drawn through the maximum slope of the shock front and the zero line.) The reason for the difference between the traces for argon and the traces for nitrogen now becomes apparent.

Figure 8 presents the wall-pressure data from several oscillograms in non-dimensional form. The time axis was non-dimensionalized by $t_{0{\cdot}05}$ and the pressure axis by the ordinate at $t = t_{0{\cdot}05}$; this ordinate was used in lieu of the asymptotic value. (It should be noted that the data were taken from oscillograms for which the sweep rate was 0·5 μsec/div.) In an approximate sense one can conclude that the process is represented by equation (1) since there are no severe departures between the different experimental curves and the curve for the boundary-layer theory. One would certainly expect the curves to depart near their respective shock-front profiles because one could not expect the shock front to scale precisely with $t_{0{\cdot}05}$ (see § 5 for a further discussion of this point). However, the different curves are close enough to one another to allow the conclusion that,

in general, the effect of the heat transfer to the cold wall depresses the pressure jump across a reflected shock front (immediately after reflexion) to about 85–90 % of the value for a thermally insulated end wall. Therefore the effect of the cold end wall on the pressure jump for a reflecting shock front is relatively small and, furthermore, its effect on the wall-pressure history for a relaxing gas can be essentially ignored for $t > t_{0\cdot05}$.

Boundary-layer theory gives a surprisingly good value for the pressure perturbation on the end wall for times as short as one or two 'shock thicknesses'. In quantitative terms, we find that the boundary-layer theory gives a good value for the wall-pressure perturbation for $p'/p_5 < 0\cdot10$, i.e. $t > 100\,\tau_{c5}$ (τ_{c5} = collision time in region 5).

4. Vibrational relaxation in carbon dioxide

It is a well known fact that the pressure is a very insensitive variable for studying the flow in the relaxing region behind a free running (or steady) shock wave in a real gas, and that the density or temperature of the flow is a far more useful quantity to record for study. However, for the case of the reflected shock wave, the wall pressure also becomes a very sensitive quantity for exhibiting relaxation effects.

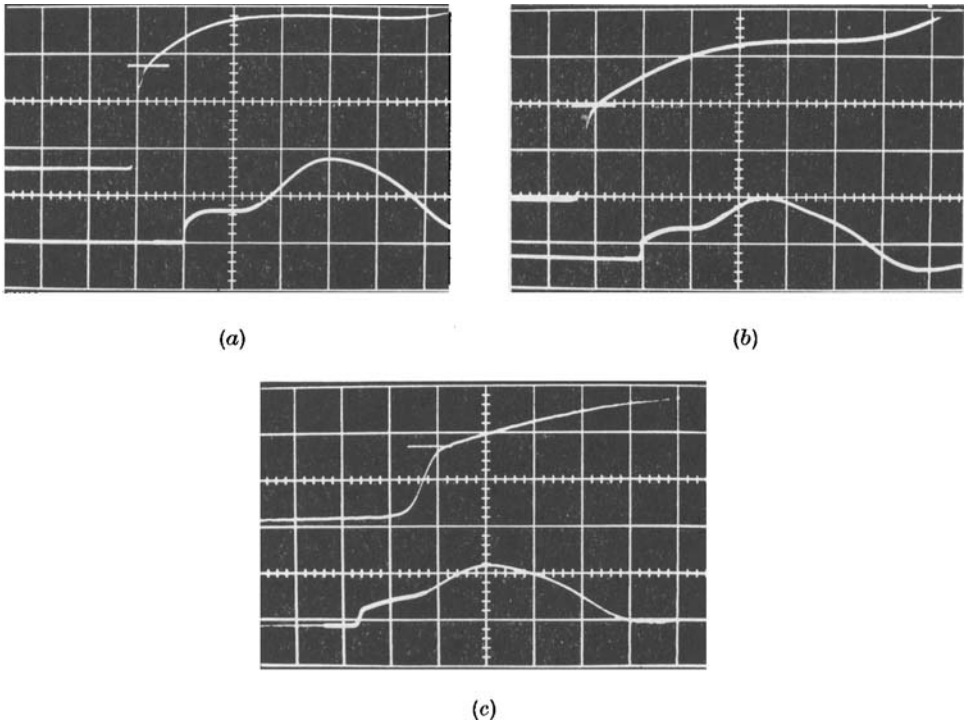

FIGURE 9. Wall-pressure history showing the effect of vibrational relaxation in carbon dioxide. (*a*) $p_1 = 3\cdot5$ mm Hg, $M_s = 4\cdot66$, $V_g = 0\cdot71$ kV; upper, 3·33 mV/div. (*b*) $p_1 = 0\cdot5$ mm Hg, $M_s = 6\cdot42$, $V_g = 2\cdot2$ kV; upper, 3·33 mV/div. (*c*) $p_1 = 0\cdot1$ mm Hg, $M_s = 7\cdot80$, $V_g = 2\cdot5$ kV; upper, 1·66 mV/div. Each oscillogram: upper, 1 μsec/div; lower, 5 μsec/div. M_s based on $\gamma = 7/5$. Horizontal mark: frozen–frozen jump.

This becomes evident from an inspection of figure 9 where several wall-pressure histories for reflected shocks in carbon dioxide are presented. The traces of figures 9(*a*) and 9(*b*) show a 'sudden' transition corresponding to a frozen jump across the viscous shock front and then a relaxation to equilibrium. At higher temperatures, the ratio of the time scale for the relaxation to the time scale for the viscous shock front is not nearly so great, and a clear separation no longer exists. Figure 9(*c*) presents a trace for which the two processes begin to merge into a single combined front. It should be noted that since the relaxation process produces such a large effect in carbon dioxide, any 'corrections' to the pressure traces, due to the heat-transfer effect considered in the above discussion, can be ignored for all practical purposes.

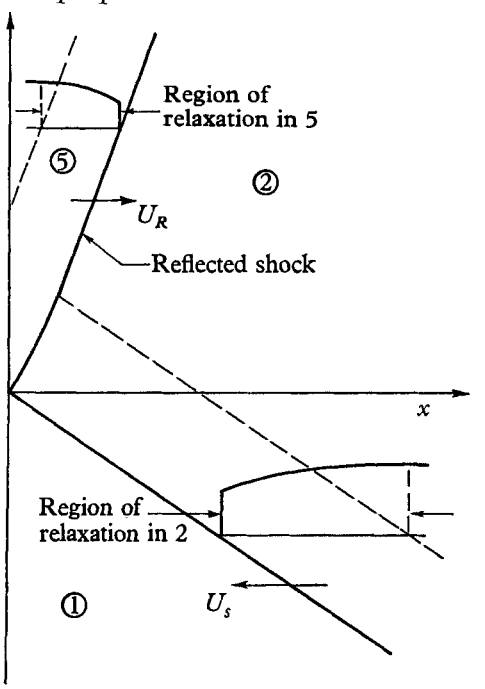

FIGURE 10. (x, t)- diagram for a reflected shock in a relaxing gas.

An inspection of the (x, t)- diagram for a reflected shock wave in a relaxing gas (figure 10) shows that there are two regions in which the gas undergoes relaxation: one behind the incident shock wave (region 2), and one behind the reflected shock wave (region 5). Therefore the reflected shock wave propagates into a region of non-uniform conditions. The flow field can be conceptually simplified by approximating the flow by a combination of two separate processes: (1) a relaxation in region 5 alone, with region 2 having uniform equilibrium conditions, and (2) the propagation of a reflected shock wave into a flow which is in the process of relaxing in region 2 but for which the gas does not undergo further relaxation in region 5.

Case (1) can be realized by suddenly setting a piston into uniform motion in a relaxing gas and viewing the piston as being the end wall in the present experiment. An analysis of this case shows that the wall pressure should decrease

slightly ($\approx 12\%$ for CO_2 and $M_s = 6$) from the initial frozen value to the final equilibrium value, somewhat as shown in figure 11 (*a*), and the wall-pressure history should exhibit a decay time τ_5 equal to an average value for the relaxation time for the gas in region 5. (Details for this case in the linearized form can be found in a paper by Spence 1961). The important conclusion is that relaxation in region 5 *decreases* the wall pressure slightly from the initial frozen value.

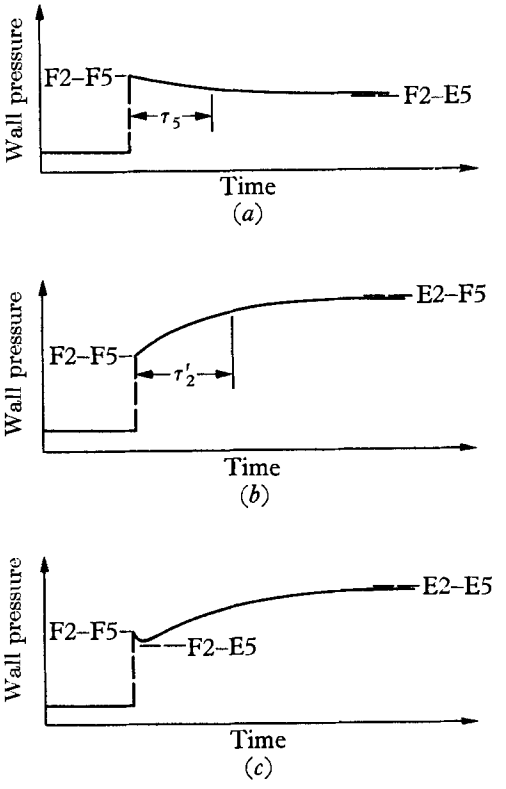

FIGURE 11. End-wall pressure history for relaxation in various regions. (*a*) Relaxation in region 5 alone; (*b*) relaxation in region 2 alone; (*c*) combined process for $\tau_5 \ll \tau_2'$.

An analysis of case (2) shows that the wall pressure should increase significantly ($\approx 70\%$ for CO_2 and $M_s = 6$) due to the non-uniform conditions in region 2; this is depicted in figure 11 (*b*). (The analysis for this case follows the argument leading to equation (4) given below.) Here the time scale for the pressure rise τ_2' is a function of the average relaxation time τ_2 for the gas in region 2 ($\tau_2/\tau_2' \approx 5$ for CO_2 and $M_s = 6$). The important conclusion is that the wall pressure is *increased considerably* over the initial frozen value due to relaxation in region 2.

The actual process is a combination of the two cases and is schematically represented in figure 11 (*c*), assuming $\tau_5 \ll \tau_2'$.† The three pressure levels, identified

† Professor N. H. Johannesen has recently obtained a computer solution for the problem of the normal reflexion of a shock from a wall, for the case of an idealized vibrationally relaxing gas, and has found a theoretical wall-pressure history similar to that given in figure 11 (*c*).

in figure 11(*c*), were computed theoretically for carbon dioxide, assuming all four vibrational modes of the molecule to be in thermal equilibrium for the initial gas and for the shocked states E2 and E5. The theoretical values together with experimental data are presented in figure 12 versus incident-shock Mach number; the two voltage jumps exhibited by the oscillogram traces for carbon dioxide were converted to pressure jumps, $(p_5 - p_1)_F$ and $(p_5 - p_1)_E$, by using the gauge calibration constant, 18·5 μV/mm Hg for a gauge voltage of 1 kV (the gauge voltage V_g is variable, $0 < V_g < 5$ kV, and was adjusted for each run so that the resulting trace would cover 2 to 3 divisions of vertical deflexion on an oscillogram).

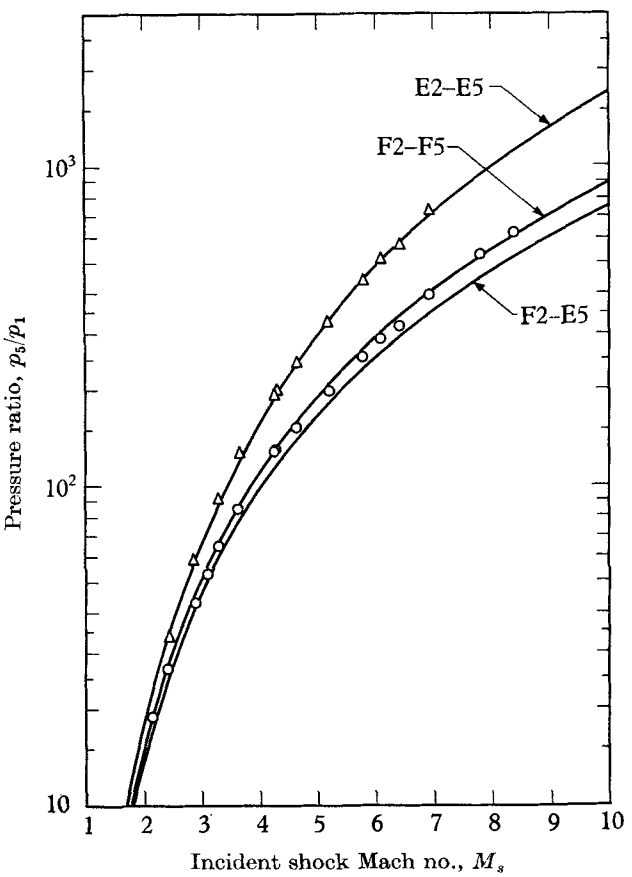

FIGURE 12. Pressure ratio across a reflected shock in carbon dioxide for jumps between various states, M_s based on $\gamma = \frac{7}{5}$. ○, pressure jump across viscous shock front; △, pressure jump at equilibrium.

The figure shows that the experimental pressure jump across the viscous shock front (denoted by circles) corresponds well to the theoretical frozen 2-frozen 5 pressure jump, and that the experimental pressure level at equilibrium (denoted by triangles) corresponds very closely to the theoretical equilibrium 2-equilibrium 5 jump. Since the dip is missing in the experimental traces, this means that $\tau_5 \approx \tau_2'$ and that figure 11(*c*) is drawn incorrectly for carbon dioxide:

the alternative case, $\tau_5 <$ shock front thickness, would require a vibrational relaxation time for carbon dioxide much shorter than the values given below.

The conclusions drawn from figures 9–12 can be summarized as follows:

(1) The experiment confirms the results obtained by Zienkiewicz, Johannesen & Gerrard (1963) and Camac (1964), where it is concluded that all four vibrational modes for the carbon dioxide molecule relax simultaneously rather than in stages as suggested by Griffith (1961).

(2) For carbon dioxide the initial slope of the wall-pressure trace is positive. Therefore information on the relaxation process taking place behind the reflected shock is not distinct from the information on the process behind the incident shock.

(3) The wall pressure is very sensitive to the flow conditions behind the incident shock and provides an experimental technique for studying the flow in that region.

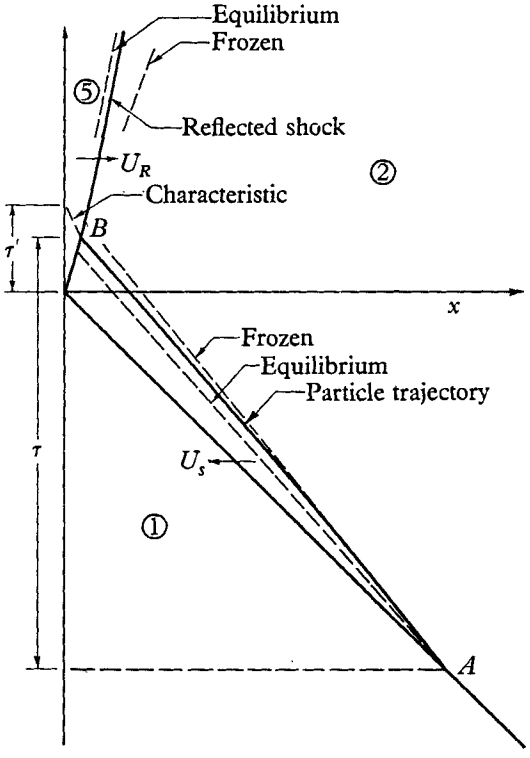

FIGURE 13. (x, t)-diagram for a reflected shock in carbon dioxide and $M_s = 5$ (approximately to scale).

The relaxation time indicated by each of the wall-pressure traces in figure 9 is therefore principally a measure of the relaxation time for the gas behind the incident shock wave. The ratio between the relaxation time τ in region 2 and the relaxation time τ' exhibited by the wall-pressure history was computed for carbon dioxide using the following simplified model for the flow field.

Figure 13 represents an (x, t)-diagram (drawn approximately to scale) for a shock wave in carbon dioxide and $M_s = 5$, and defines the relevant quantities in

the flow field. For very short times the particle trajectory in region 2 can be approximated with the frozen speed, and for very long times it can be approximated with the equilibrium speed. However, for a time equal to the relaxation time in region 2, a reasonable approximation is the average between the two speeds. Similar reasoning holds for the trajectory of the reflected shock wave. (Note that here we are using the condition $\tau_5 \approx \tau_2'$, obtained above.) The state of the gas at the terminal end of the particle trajectory in region 2 (point B in the figure) is such that its temperature is lower and its density and particle speed are greater than the corresponding quantities at the initial point of the trajectory (point A). Each of these factors contribute to the strengthening of the reflected shock wave at B. Therefore a positive pressure wave is produced at the shock and propagates back towards the end wall along a characteristic in region 5; the resulting pressure history on the end wall then gives τ'. The appropriate average velocities and geometrical relations were then used to compute the ratio τ/τ' for various incident-shock Mach numbers.

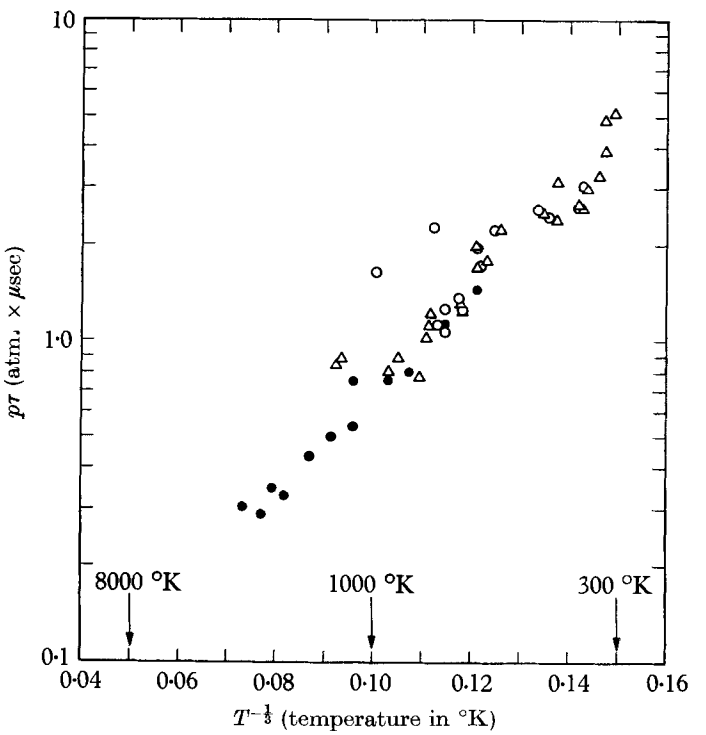

FIGURE 14. Vibrational relaxation time in carbon dioxide. ●, Present results; ○, Blackman (1956); △, Griffith *et al.* (1956)

This ratio was found to range between $\tau/\tau' \approx 4{\cdot}5$ for $M_s = 4$ and $\tau/\tau' \approx 6$ for $M_s = 10$. The ratio was then used to convert the relaxation time given by an oscillogram (based on a $1/e$ type definition) to the value for the gas in region 2. The results of the experiment are presented in figure 14 along with the data obtained by Blackman (1956) and Griffith, Brickl & Blackman (1956). The present data were plotted, as is the usual procedure, using the average temperature

and pressure in region 2 (average of the values for the frozen state immediately behind the incident shock and the equilibrium state downstream of the incident shock).

Although the vibrational relaxation time for carbon dixoide as determined by the present experiment agrees well with previously determined values, figure 14 is not being presented *primarily* as additional information on the vibrational relaxation time in carbon dioxide (since the computation for the ratio τ/τ' may need refinement); but rather, *primarily*, to show that the present experimental technique complements the available information on relaxation time in carbon dioxide. That is, the present method permits one to obtain data for higher temperatures than can be obtained using a conventional optical interferometer. (This is due to a sensitivity limitation which restricts the use of the optical interferometer to densities greater than the density corresponding to a pressure of 1 mm Hg and a temperature of 300 °K.)

The use of a shock wave for the experimental determination of the relaxation time in a gas must, for purposes of simplicity, be restricted to the Mach-number range (or temperature range in region 2) for which the relaxation length behind the shock is greater than roughly ten times the thickness of the viscous shock front. An example of the upper limit for vibrational relaxation in carbon dioxide is presented in figure 9(*c*) where $M_s \approx 8$ and $T^{-\frac{1}{3}} \approx 0{\cdot}07$. Therefore the plot of figure 14 can not be easily extended experimentally below, say $T^{-\frac{1}{3}} \approx 0{\cdot}06$ using a shock wave. Consequently, the present experimental method covers the range in temperatures between this upper limit and the limit for an interferometer.

Of course, for different gases the maximum temperature (or Mach number) is different. However, the structure of the relaxation at the upper limit can always be resolved by the present method since, as will be seen in the following section, the profile of the viscous shock front itself can be observed with the pressure gauge.

With regard to the present experimental method, two items warrant special emphasis:

(1) The extreme sensitivity of the wall pressure to the conditions of the flow behind the incident shock wave as observed in the present experiment, is *not unique to carbon dioxide alone*. It is quite easy to show that, *regardless of the type of relaxation involved*, the wall pressure changes by practically the same ratio as the density change behind the incident shock; and it is well known that ρ_2 is quite sensitive to relaxation. This can be seen as follows. The continuity and momentum equations can be solved to give the following (exact) jump relations for the incident and reflected shocks (velocities referred to laboratory co-ordinates)

$$\left.\begin{aligned} p_5 - p_2 &= \rho_5 u_2 U_R, \\ u_2/U_s &= (\eta-1)/\eta, \\ U_R/U_s &= (\eta-1)/(\zeta-\eta), \end{aligned}\right\} \tag{2}$$

where $\eta = \rho_2/\rho_1$ and $\zeta = \rho_5/\rho_1$. Substituting into the first expression, we obtain

$$(p_5 - p_2)/\rho_1 U_s^2 = \frac{\zeta}{\zeta-\eta}\frac{\eta-1}{\eta}(\eta-1) \approx (\eta-1). \tag{3}$$

The error introduced by the last step is at most 15 % and decreases considerably for $M_s > 1$ and $\gamma < \frac{7}{5}$. Dividing the equilibrium value (E) by the frozen value (F), we obtain the approximate relation

$$(p_5)_E/(p_5)_F \approx (\rho_2)_E/(\rho_2)_F, \tag{4}$$

which shows that the wall-pressure changes by roughly the same ratio as the density change behind the incident shock wave for any relaxing flow, i.e. vibration, dissociation, or ionization.

(2) The details concerning the initial slope of the wall-pressure history should be investigated theoretically for a general relaxing gas to determine the relationship between the initial slope and the relaxation times in regions 2 and 5. This is of particular interest since the experimental method shows great promise in providing accurate information on relaxation times in different gases at high temperatures.

5. Wall pressure for a reflecting shock front

Some examples of wall-pressure profiles for reflecting shock fronts are presented in figure 15. The initial pressure (the most sensitive scaling quantity) is common (50 μ Hg) for all three traces presented in the figure.

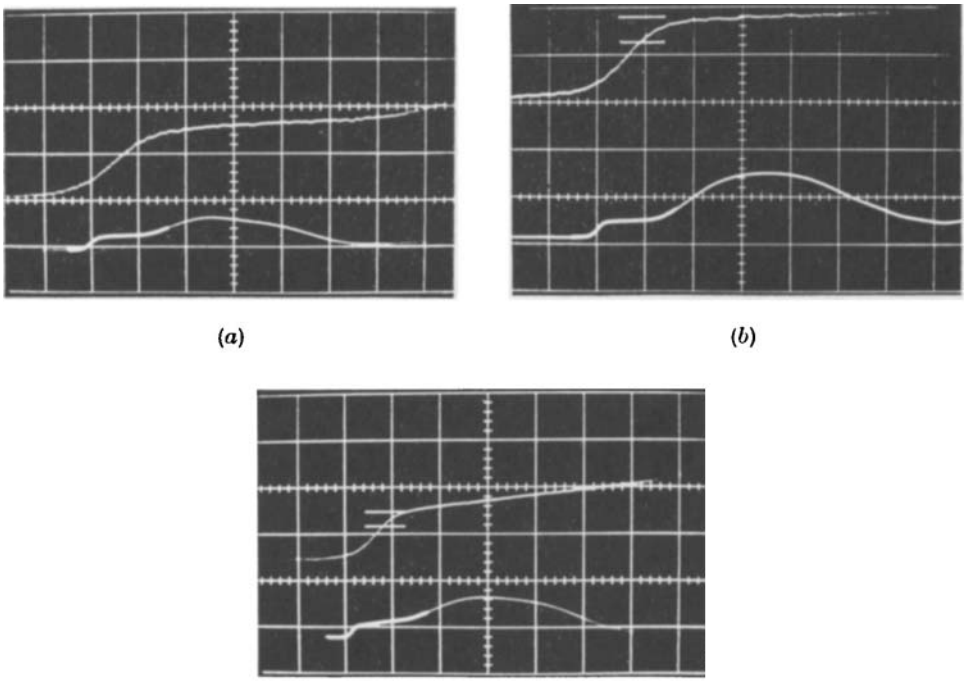

FIGURE 15. p_{xx} profile for a reflecting shock front, $p_1 = 50\ \mu$ Hg. (*a*) Argon, $M_s = 7{\cdot}32$; (*b*) nitrogen, $M_s = 6{\cdot}41$; (*c*) carbon dioxide, $M_s = 8{\cdot}25$ (based on $\gamma = \frac{7}{5}$). Each oscillogram: upper, 1 μsec/div; lower, 5 μsec/div. Upper mark, $\gamma = \frac{7}{5}$; lower mark, $\gamma = \frac{5}{3}$.

For a low-Reynolds-number flow such as the normal reflexion of a shock front, the normal stress experienced by a pressure gauge does not correspond to the mean stress p but to the normal component of the stress tensor p_{xx}, i.e.

$$p_{xx} = -p + \tau_{xx},$$

which for one-dimensional flow reduces to

$$p_{xx} = -p + \tau.$$

Therefore the wall-pressure profiles presented in figure 15 are profiles of p_{xx} rather than profiles of the mean stress p. However, on both sides of the shock front the viscous stress τ approaches zero quite rapidly, and the stress tensor p_{xx} and the mean stress p become equal. Therefore, immediately behind the shock front an ordinate on the p_{xx} profile can be compared directly to the mean stress as was done above.

It is well known that the pressure ratio p_5/p_1 is quite sensitive to changes in the ratio of specific heats γ. Therefore, if a diatomic gas were not fully relaxed rotationally within the reflected shock front, then the value of the wall-pressure jump across the reflected shock would lie between the values for a monatomic and a diatomic gas and the change in the wall-pressure jump should be measurable experimentally. The wall-pressure jumps corresponding to $\gamma = \frac{5}{3}$ and $\gamma = \frac{7}{5}$ (assuming a constant incident shock speed) are displayed as horizontal marks on the traces for nitrogen and carbon dioxide in figure 15. These values were computed and plotted for a thermally insulated wall, and do not include a correction (decrease) of about 10 % (according to the results of § 3) to account for the effect of heat transfer to the end wall in the experiment. Figures 15(*b*) and 15(*c*), which are typical of all of the profiles obtained with nitrogen and carbon dioxide in the present experiment, show that both molecules are fully relaxed rotationally within the reflected shock front profile. This is in agreement with previous investigations on the density jump across the incident shock front in nitrogen (Linzer & Hornig 1963) and carbon dioxide (Camac 1964).

The following discussion will be restricted to the usual gross description of shock profiles, i.e. the profile for a reflecting shock front will be described by its maximum slope thickness, defined in the usual way. If we define Δt to be the maximum slope thickness as displayed by an oscillogram of the wall pressure, U_s the incident shock velocity, and λ_1 the mean-free-path length for the initial gas, then a straightforward argument, using the non-steady one-dimensional Navier–Stokes equations, shows that the dimensionless ratio

$$\lambda_1/\delta = \lambda_1/\Delta t U_s \tag{5}$$

is a function of incident Mach number alone, provided the Prandtl number Pr and the viscosity ratio μ/μ_1 are functions of the temperature ratio T/T_1 alone.

Figure 16 represents a plot of the reciprocal thickness λ_1/δ for a reflecting shock front, as defined by equation (5), versus the incident Mach number for the experimental data for argon, nitrogen and carbon dioxide. The maximum slope thicknesses for the carbon dioxide data were obtained by using the portion of the

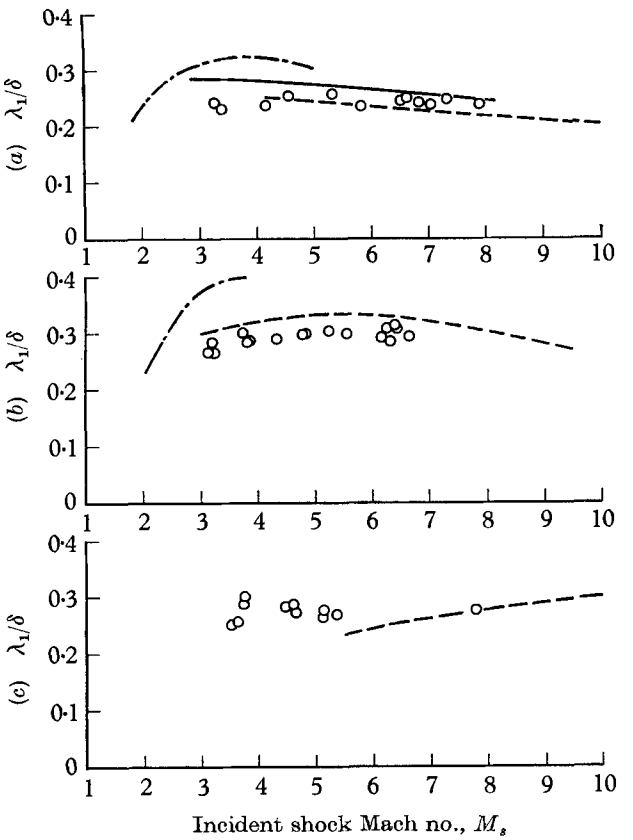

FIGURE 16. Reciprocal shock thickness for a reflecting shock front. (*a*) Argon; (*b*) nitrogen; (*c*) carbon dioxide (M_s based on $\gamma = \frac{7}{5}$). ——, Average of Russell data; – – –, average of Camac data; — – —, average of Linser & Hornig data (the data are for the *density* profile of the *incident* shock front).

profile that corresponded to the frozen–frozen pressure jump. The mean-free-path length λ_1 was computed from the relation

$$\lambda = \frac{16}{5}\frac{\mu}{\rho a}\sqrt{\frac{\gamma}{2\pi}}$$

for all three gases, using the respective room temperature values for the viscosity, density, and speed of sound.

Lest a casual inspection of figure 16 leads one to believe that the measured reciprocal thicknesses are a property of the pressure gauge rather than a valid gas dynamic effect, it should be pointed out that the experimental data involved a variation in λ_1 of a factor of four and a variation in U_s of a factor of almost three.

A comparison of the reciprocal thickness for the nitrogen data with that for the argon data shows that the value of λ_1/δ for nitrogen is roughly 21% greater than that for argon. This is in rough agreement with the measurements reported by Linzer & Hornig (1963) on the value of λ_1/δ for the density profile for a free-run-

ning shock wave in nitrogen and argon; their data indicate a reciprocal thickness for nitrogen approximately 30 % greater than that for argon (see figures 4 and 5 of Linzer & Hornig 1963).

It is also noteworthy that there is no striking difference in the thickness between a polyatomic gas like carbon dioxide and a monatomic gas like argon. This result is significant because it indicates that, from a gas dynamic point of view, there are no great differences between the transport properties of carbon dioxide and the transport properties of a simple (from the kinetic theory point of view) gas like argon. This result is in contrast to some of the early thoughts on the *maximum-slope thickness* for a shock wave in carbon dioxide (Gilbarg & Paolucci 1953), where the effect of vibrational relaxation was incorporated into the bulk viscosity for the gas; this leads to a predicted *maximum-slope thickness* three orders of magnitude greater than the present measurements.

In § 3 it was found that the effect of the cold end wall depresses the pressure jump across the reflected shock front (immediately after reflexion) by 10 % below the theoretical thermally insulated case. If the experiment for the case of the thermally insulated end wall were physically possible, or theoretical computations were available, then the results for the maximum-slope thickness for the two cases could be compared to determine the extent to which the heat transfer to the end wall alters the profile thickness. However, in lieu of this one can resort to a much cruder comparison by using available information on the incident shock front (λ_1/δ for the *density* profile). It is quite interesting to compare the present data for argon, nitrogen and carbon dioxide (figure 16) with the respective data for the incident shock obtained by Russell (1965), Linzer & Hornig (1963), and Camac (1963, 1964). The close similarity between the results for the two apparently different processes is perhaps surprising.

A question of interest in the study of the material of § 3 is whether or not, by changing test conditions (initial pressure, Mach number, etc.), it is possible to change appreciably the ratio of the time scale for the effect of the cold wall to the time scale for the reflecting shock front, i.e. to make the shock front appear as a discontinuity on the time scale of interest for the study of the effect of the cold wall. It can now be shown, in an approximate sense, that the ratio of the characteristic time scale for the effect of the heat transfer τ_{HT} to the characteristic time scale for a reflecting shock front τ_{SF} is *essentially* fixed for a given gas and cannot be *greatly* increased over the values displayed by the wall-pressure traces of figures 5 and 6. If we ignore the weak Mach-number dependence in equation (1), we can write

$$\tau_{HT} \sim \mu_5/\rho_5 a_5^2.$$

For the Mach number range exhibited by figure 16, the value of λ_1/δ is essentially a constant for each gas and we can write, using equation (5),

$$\tau_{SF} \sim \lambda_1/U_s.$$

We then have for the ratio of time scales

$$\tau_{HT}/\tau_{SF} \sim (\mu_5/\mu_1)\, M_s/(p_5/p_1).$$

If we assume the viscosity ratio can be represented by a power law in the temperature ratio

$$\mu_5/\mu_1 \sim (T_5/T_1)^{\omega},$$

where $\frac{1}{2} < \omega < 1$, and since for large Mach number

$$T_5/T_1 \sim p_5/p_1 \sim M_s^2,$$

we then have for the ratio of time scales

$$\tau_{HT}/\tau_{SF} \sim M_s^{2\omega-1}. \tag{6}$$

Therefore the ratio of time scales does not depend on a quantity like initial pressure where a very large factor could be introduced, but rather on something like the square root of the Mach number, from which one could only hope to obtain a factor of 2 or 3 over the ratio displayed by figures 5 and 6. It should be noted that equation (6) is only being used for a rough estimation of the scaling; a more precise value would have to be obtained from the full equations, without the approximations employed above.

The author wishes to express his sincere appreciation to Prof. H. W. Liepmann and Prof. A. Roshko for suggesting the study of the shock reflexion process and for their willingness to discuss problems which arose in the investigation.

The experiments conducted in the GALCIT 17 in. diameter low-pressure shock tube were supported by the National Aeronautics and Space Administration.

REFERENCES

Amdur, I. & Mason, E. A. 1958 *Phys. Fluids*, **1**, 370.

Baganoff, D. 1964 *Rev. Sci. Instr.* **35**, 288.

Blackman, V. 1956 *J. Fluid Mech.* **1**, 61.

Camac, M. 1963 *AVCO-Everett Res. Lab. Res. Rep.* no. 172.

Camac, M. 1964 *AVCO-Everett Res. Lab. Res. Rep.* no. 194.

Clarke, J. F. 1962 *J. Fluid Mech.* **13**, 47.

Gilbarg, D. & Paolucci, D. 1953 *J. Rat. Mech. Anal.* **2**, 617.

Goldsworthy, F. A. 1959 *J. Fluid Mech.* **5**, 164.

Griffith, W., Brickl, D. & Blackman, V. 1956 *Phys. Rev.* **102**, 1209.

Griffith, W. C. 1961 *Fundamental Data obtained from Shock-Tube Experiments* (ed. A. Ferri, pp. 242–59. New York: Pergamon Press.

Liepmann, H. W. & Bowman, R. M. 1964 *Phys. Fluids*, **7**, 2013.

Liepmann, H. W., Roshko, A. Coles, D. & Sturtevant, B. 1962 *Rev. Sci. Instr.* **33**, 625.

Linzer, M. & Hornig, D. F. 1963 *Phys. Fluids*, **6**, 1661.

Russell, D. A. 1965 *Rarefied Gas Dynamics* (ed. J. H. de Leeuw,). New York: Academic Press (to be published).

Spence, D. A. 1961 *Proc. Roy. Soc.* A, **264**, 221.

Sturtevant, B. & Slachmuylders, E. 1964 *Phys. Fluids*, **7**, 1201.

Zienkiewicz, H. K., Johannesen, N. H. & Gerrard, J. H. 1963 *J. Fluid Mech.* **17**, 267.